J. Appl. Cryst. (1997). **30**, 722–726

Studying the Microstructure of Unaged and Aged PVDF by Small- and Wide-Angle X-ray Scattering

NORBERT STRIBECK[a]* AND STEFAN BUCHNER[b]

[a] *Institut für Technische und Makromolekulare Chemie, Universität Hamburg, 20146 Hamburg, Germany, and* [b] *Shell Research & Technology Center, 1030 BN Amsterdam, The Netherlands. E-mail: stribeck@vxdesy.desy.de*

(*Received 23 July 1996; accepted 28 January 1997*)

Abstract

A layer from plasticized poly(vinylidene fluoride) (PVDF) was aged by exposing one of its faces to an aggressive fluid at elevated temperature and pressure. From visual inspection the aged material appeared not to be homogeneous. Therefore, samples from three distinguishable regions were compared with a sample cut from the virgin material by studying their small- and wide-angle X-ray scattering (SAXS and WAXS). The results show that plasticizer has vanished from the aged material, the crystalline layer thickness distribution has narrowed, amorphous lamellae are collapsed and voids have been created. Within the aged material the number of voids varies: there are more at the inner surface and fewer at the outer surface beneath the rods of a supporting metal grid. Based on the results of this study and theoretical considerations, a method for the quantitative description of the ageing process is proposed, which only requires a simple kind of SAXS measurement.

1. Introduction

Permeability and mechanical properties of semi-crystalline polymers depend on the manner in which the crystalline and amorphous domains are organized. It is well known that these properties may deteriorate during the technical use of such materials and thus limit their service life. Some polymers like poly(vinylidene fluoride) (PVDF) lack processability if no plasticizer is added. Since the plasticizer is somewhat volatile, its content may decrease during the lifetime of the material and thus contribute to its ageing.

Although ageing has been extensively investigated with respect to material properties, transport characteristics (Yampol'skii *et al.*, 1993) have not often been studied. The relation of ageing to morphological features has been established several times (Montserrat & Cortes, 1995; Johansson & Tegenfeldt, 1993; Arnold, Leo & Tarjani, 1988), but to our knowledge no study of the ageing of PVDF has been reported.

2. Experimental

2.1. *Material*

PVDF is a semi-crystalline polymer with good chemical resistance. It is frequently used as a permeation barrier to aggressive fluids. The basis for interest is its use in flexible pipelines or linings within steel pipes. The studied commercial-grade material contains 12 wt% ($\Phi_{pl} = 0.12$) of sebacic acid dibutyl ester. The plasticizer ensures extrudability and flexibility.

The material was aged in an environment of methane gas containing organic and inorganic condensates in which a polymer layer of 8 mm thickness was pressed against a supporting metal grid. The fluid pressure was 8 MPa and temperature 353 K. The material face supported by the metal grid was exposed to ambient pressure. Visual inspection of the aged material shows its inhomogeneity (Fig. 1). Three samples from distinguishable regions were compared to a sample cut from the virgin material. Measurements were reproduced several times from different samples (twice for the aged sample in the ageing process described here, many times for virgin samples).

For the purpose of the X-ray studies, slices of 0.600 (3) mm thickness were sectioned using a Buehler ISOMET^{TM} low-speed saw.

2.2. *Methods*

Densities of the samples were determined in a density gradient from CCl_4 and 1,3-dibromopropane.

Wide-angle X-ray scattering (WAXS) and SAXS patterns were recorded on photographic film using a

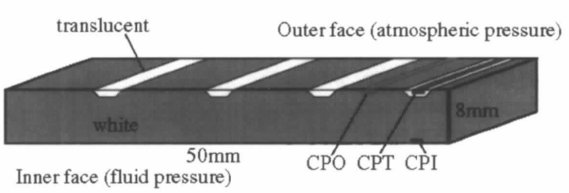

Fig. 1. Aged PVDF material. During the ageing process metal bars covered the translucent regions of the material. Positions of three studied samples from the translucent (CPT) region, the outer face (CPO) and the inner face (CPI) of the white body are indicated.

pinhole camera. Further SAXS experiments were performed using a Kratky camera equipped with a proportional detector and energy discriminator. A moving slit device (Stabinger & Kratky, 1978) served for calibration of absolute intensity and for determination of the sample absorption.

3. Data evaluation

3.1. *Evaluation of discrete scattering neglecting void scattering*

Kratky camera data were quantitatively evaluated using the method of interface distribution analysis (Ruland, 1977) and a generalized model for stacking statistics (Stribeck, 1993). After subtraction of the apparent background the measured intensity in absolute units, $\tilde{I}(s)/V$, is transformed into an 'interference function', $\tilde{G}_{id}(s)$, of the ideal two-phase system

$$\tilde{G}_{id}(s) = [\tilde{I}(s)/V - \tilde{I}_{Fl}/V]s^3/[(1 - 8\pi^2\sigma_i^2 s^2)\,\mathrm{erfc}(2\pi\sigma_i s) + 4(\pi\sigma_t s)^{1/2}\exp(-4\pi^2\sigma_t^2 s^2)] - \tilde{A}_P. \quad (1)$$

In this function deviations according to the nonideal nature of the two-phase system are eliminated by consideration of a fluctuation background $\tilde{I}_{Fl}/V$ as well as the width of the transition zone $d_t = 3\sigma_t$ at the interface between the crystalline and the amorphous layer (for details see Stribeck, 1993). Reverse transformation of this function yields

$$\tilde{I}_{id}(s)/V = (1/s^3)[\tilde{G}_{id}(s) + \tilde{A}_P], \quad (2)$$

the slit-smeared intensity corresponding to the ideal two-phase system. Finally, a Fourier–Bessel transformation of $\tilde{G}_{id}(s)$ yields

$$g_1(x) = \pi \int_0^\infty \tilde{G}_{id}(s)[4J_0(2\pi xs) - 2(2\pi xs + 1/2\pi xs)J_1(2\pi xs)]\,\mathrm{d}s \quad (3)$$

the interface distribution function (IDF), $g_1(x)$. This is proportional to the second derivative of the one-dimensional correlation function (Vonk & Kortleve, 1967). The IDF is composed from a series of distance distributions, $h_i(x)$. The centres of gravity of the first two distance distributions, $\bar{d}_1$ and $\bar{d}_2$, represent the average thicknesses of the layers of 'phase 1' and 'phase 2', respectively. Assuming 1D stacking statistics (Hermans, 1944) the IDF can be represented only using $h_1(x)$ and $h_2(x)$. Thus a model IDF can be fitted to the measured data. The parameters of the model are the thicknesses of the crystalline and the amorphous layers, $\bar{d}_c = \bar{d}_1$ and $\bar{d}_a = \bar{d}_2$, the relative widths $\sigma_c/\bar{d}_c$ and $\sigma_a/\bar{d}_a$ of the distance distributions (which are assumed to be Gaussian), a parameter σ_H which serves to skew the Gaussians and finally the integral of the IDF, W. The observed relative width of the thickness distribution $h_i(x)$ is a function of both $\sigma_i/\bar{d}_i$ and σ_H, and can be computed (Stribeck, 1993) from

$$[(\sigma_i/\bar{d}_i)^2_{obs} + 1] = [(\sigma_i/\bar{d}_i)^2 + 1](\sigma_H^2 + 1), \quad (4)$$

if the effects of multiple and void scattering on the measured SAXS curve are negligible.

Table 1. *Densities of unaged (CPvi) and aged PVDF samples as measured in a density gradient tube*

Sample	ρ (g cm^{-3})	Sample	ρ (g cm^{-3})
CPvi	1.640 (4)	CPO	1.674 (4)
CPT	1.691 (2)	CPI	1.625 (3)

3.2. *Detecting void scattering*

It is assumed that void scattering, as a function of the scattering angle, decreases monotonically. Therefore it is predominant in the vicinity of zero scattering angle. The same is true for multiple scattering. If multiple scattering can be excluded, following the method proposed by Perret & Ruland (1971), it is only necessary to discriminate void scattering from the discrete SAXS of the lamellar two-phase system.

In the case of discrete scattering arising from a system of stacked, flat and extended lamellae, Stribeck (1996) has extended the treatments of Zernike & Prins (1927) and Blundell (1978) to develop an analytical expansion of the '1D slit-smeared scattering intensity' $\tilde{I}_1(s)/V = s\tilde{I}_{id}(s)/V$ about zero scattering angle,

$$\tilde{I}_1(s)/V = (\bar{d}_P/2)\Delta\rho_{el}^2 v(1-v)[(\sigma_1^2/\bar{d}_1^2) + (\sigma_2^2/\bar{d}_2^2)] + [\Delta\rho_{el}v(1-v)L]^2 s + O(s^3) \quad (5)$$

which can be used to discriminate between void scattering and discrete SAXS. Here $\bar{d}_P = \bar{d}_1\bar{d}_2/(\bar{d}_1 + \bar{d}_2)$ is the 1D equivalent of the average chord length, $\Delta\rho_{el}$ is the electron density difference between the crystalline and the amorphous phase, v is the volume crystallinity, and $L = \bar{d}_1 + \bar{d}_2$ is the long period of the layer stack. The scattering power $Q_{id} = \pi\int_0^\infty \tilde{I}_1(s)/V\,\mathrm{d}s$ of the sample is proportional to the area under the curve. The initial slope of the curve is positive and a function of the stacks composition, but not of its disorder. Unfortunately the resulting parameter values of an IDF analysis may be shifted due to surface roughness (Ruland, 1987; Semenov, 1994) of the layers. This means that a disagreement between IDF analysis and measured initial slope is not sufficient to prove void scattering. If the measured initial slope of $\tilde{I}_1(s)/V$ is negative, void scattering is probably present.

4. Results and discussion

4.1. *Density*

The measured densities of the samples are presented in Table 1. A volume crystallinity $\alpha_c = 0.45$ is computed for the virgin material CPvi.

Table 2. *Parameter values describing the nonideal two-phase system (density fluctuation background $\tilde{I}_{Fl}/V$, width of the phase transition layer d_t) and values for the slit-smeared Porod's asymptote, $\tilde{A}_P$, determined from deviations of Porod's law*

Sample	$\tilde{I}_{Fl}/V$ (e.u. nm^{-4})	d_t (nm)	$\tilde{A}_P$ (e.u. nm^{-7})
CPvi	990 (3)	0.6 (1)	18.0 (5)
CPT	365 (10)	0.3 (2)	9.5 (3)
CPO	385 (15)	0.7 (2)	9.6 (3)
CPI	371 (10)	0.7 (2)	9.3 (7)

4.2. *2D X-ray patterns*

Both WAXS and SAXS measurements exhibit the scattering of unoriented samples. All the SAXS patterns look similar. Since the differences among the WAXS patterns of all the samples are small, the patterns are not presented. To a first approximation, the ageing process appears not to affect the crystalline phase.

4.3. *Multiple scattering test*

All samples were tested for multiple scattering. After multiplication by the inverse absorption factor, all curves show an undistorted primary beam profile and therefore multiple scattering is considered to be negligible.

4.4. *Absolute SAXS with the Kratky camera*

4.4.1. *'1D' scattering curves and the ideal two-phase system.* Fig. 2 shows measured curves of the PVDF samples after the corrections according to (1) and (2), which lead to Porod's law of an ideal two-phase system. Table 2 shows the parameter values determined in the correction process. The virgin sample CPvi shows three times the fluctuation background and double the Porod's asymptote as compared with the aged samples. Because all the aged samples show the same Porod's asymptote, their scattering curves are identical for $s > 0.07\,\mathrm{nm}^{-1}$.

4.4.2. *Void scattering in the white samples.* The initial slope of the scattering curves for the white samples is negative, indicating strong void scattering. Since all the aged samples data fit the same Porod's law, it is meaningful to compare the hatched fractions in Fig. 2 by subtracting the scattering of the aged translucent sample from each of the aged white samples. The result is shown in Fig. 3.

The residual scattering intensities of the aged white samples CPO and CPI are an identical shape and the hatched areas in Fig. 2 appear to originate from mere void scattering. Only the amount of void scattering differs. If it is assumed that there are no voids in sample CPT, then void scattering at the inner face of the aged material is a factor of 4.5 higher than at the outer face in the gap between the supporting rods.

Therefore the slope of the slit-smeared one-dimensional scattering intensity appears to be an appropriate measure for the ageing of plasticized PVDF. Hence a simple procedure to study the progress of ageing can be proposed, as only the recording of the central part of the SAXS curve is necessary to obtain the required number.

4.4.3. *IDF analysis for the translucent samples.* According to the previous considerations it is only meaningful to analyze the IDF from the translucent samples and to extract the layer thickness distributions of the lamellar stacks. The corresponding curves, their fits with the one-dimensional stacking model and three-layer thickness distributions are shown in Figs. 4 and 5. Both IDFs show an ensemble of layer stacks with only short-range order, since the curves vanish for $x > 25$ nm. They do not vanish at $s = 0$. From this observation it is concluded that the layer surfaces are rough. Only in the case of the aged

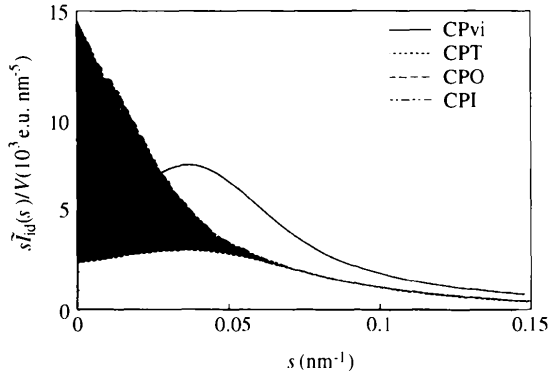

Fig. 2. One-dimensional SAXS curves $s\tilde{I}_{id}(s)/V = \tilde{I}_1(s)/V$ of unaged and aged PVDF. The area under the curve is proportional to the scattering power Q_{id} of the samples. The hatched areas show the residuals between the aged translucent sample, CPT, and the aged and white samples, CPO and CPI, respectively. Linear extrapolation covers the interval from $s = 0$ to $s = 4.2 \times 10^{-3}\,\mathrm{nm}^{-1}$.

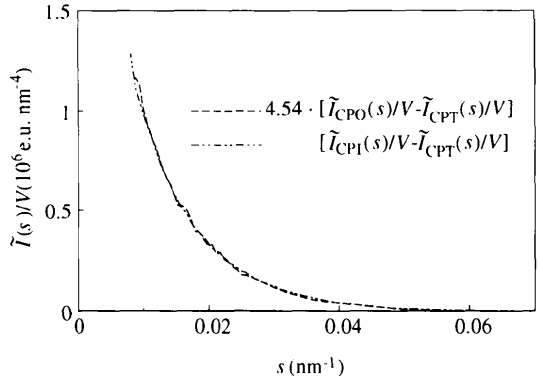

Fig. 3. After subtraction of the aged translucent sample, the residual scattering intensities of the aged white samples show the same shape.

sample CPT can the surface roughness effect be separated from the effect of the layer stack, whereas in the case of the virgin sample the peak of the crystalline thickness distribution and that of the surface roughness are too broad to be separated.

The assignment of the first distance distribution to the crystalline thicknesses relies on the crystallinity computed from density and on the assumption that no amorphous material is present outside the layer stacks. Comparison of Figs. 4 and 5 shows that ageing narrows the frequency distribution of the crystalline layer thicknesses. For the CPvi sample, the crystalline thickness distribution could not be separated from the surface roughness effect. It can be concluded that the crystalline layer thickness decreased during the ageing process. The amorphous thickness distribution, as a result of ageing, appears to broaden and shifts towards smaller thicknesses. In Figs. 4 and 5 the weight W of the IDF is the area shown in grey. It is the integral over the whole IDF as computed by the model-fitting procedure. It is smaller for the aged sample than for the virgin one. Part of the reduction can be attributed to the separation of surface roughness, but comparison of samples CPvi and CPT in Fig. 2 reveals further evidence: the scattering power of the aged sample has decreased considerably due to a reduction of plasticizer content in the aged sample. The information which is qualitatively shown in Figs. 4 and 5 is presented quantitatively in Table 3. Assuming for an ideal layer stack $W/2 = \tilde{A}_P$, comparison with Table 2 reveals that there is good agreement with the CPvi sample, since surface roughness could not be separated. For the CPT sample the surface roughness contributes to the shape of the scattering curve in the Porod's region $[\tilde{I}_{id}(s)/V = \tilde{A}_P/s^3]$ by 50% in units of $\tilde{A}_P$. The number for the average crystalline thickness $\bar{d}_c$ is not changed by the ageing process, but a true decrease appears to be more likely. For the average amorphous layer thickness, a decrease is observed as a result of ageing, since the plasticizer has vanished during the ageing process, causing a shrinkage of amorphous layers.

Table 3. *Parameter values obtained by fitting the IDFs of the translucent samples with the stacking model*

Estimated errors of the fit are computed from the parameter correlation matrix output by the nonlinear regression program. Observable relative variances in the bottom are computed using equation (4).

	CPvi	CPT
W (e.u. nm^{-7})	36.0 (2)	10.1 (1)
$\bar{d}_c$ (nm)	4.2 (1)	4.2 (1)
$\bar{d}_a$ (nm)	9.0 (5)	7.6 (1)
$\sigma_c/\bar{d}_c$	0.71 (3)	0.16 (1)
$\sigma_a/\bar{d}_a$	0.37 (3)	0.47 (2)
σ_H	0.32 (4)	0.41 (1)
$(\sigma_c/\bar{d}_c)_{obs}$	0.81	0.45
$(\sigma_a/\bar{d}_a)_{obs}$	0.50	0.65

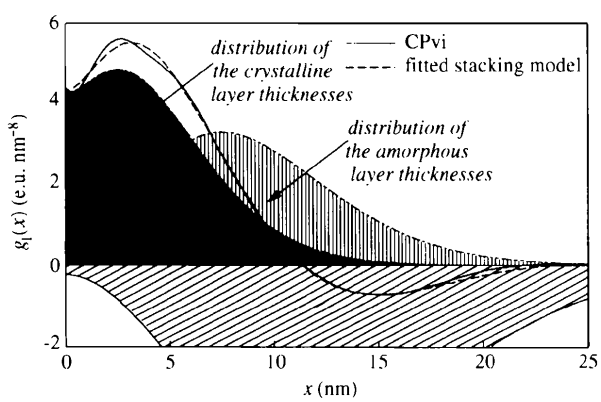

Fig. 4. IDF of the virgin PVDF sample (CPvi), its fit and decompostion into the series of the layer thickness distributions utilizing layer-stacking statistics. In the vicinity of $x = 0$, surface roughness of the layers contributes to the IDF and cannot be separated from the 'true' layer thickness distributions.

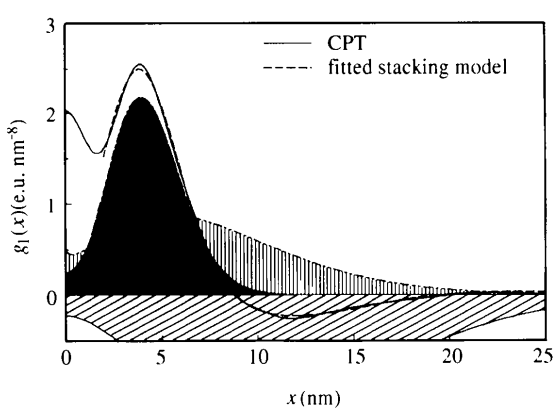

Fig. 5. IDF of the aged translucent PVDF sample (CPT), its fit and decomposition into the series of the layer thickness distributions utilizing layer-stacking statistics. In the vicinity of $x = 0$, surface roughness of the layers contributes to the IDF, but can be separated from the 'true' layer thickness distributions.

For the virgin sample the volume crystallinity computed from density (45%) is higher than the crystallinity computed from the parameters of the IDF analysis (32%). Several reasons for this can be considered. First, the value computed from density relies on the accuracy of the initial plasticizer content, determined by the PVDF supplier. Second, the average crystallite thickness of sample CPvi is underestimated in the IDF analysis because of the present roughness of the domain surfaces.

4.4.4. *Scattering power and contrast.* Evidence for the loss of plasticizer during the ageing process is given by comparing the scattering powers Q_{id} of both the virgin and the aged translucent samples. By integrating $Q_{id} = \pi \int_0^\infty \tilde{I}_1(s)/V \, ds$, values of 4330 and 2190 e.u. nm^{-6} are obtained for the CPvi and CPT samples, respectively.

Under the assumption that the whole sample volume is filled with layer stacks, the relation $Q_{id} = \Delta\rho_{el}^2 v(1-v)$ is valid. Thus one can compute $\Delta\rho_{el}$, the density difference between the amorphous and the crystalline phase, from the scattering power and compare it to the expected value derived from the densities of both the phases, $\Delta\rho_{el,CPvi} = 141$ e.u. nm^{-3} and $\Delta\rho_{el,CPT} = 97$ e.u nm^{-3}, respectively. Using the densities cited in §2.2, $\Delta\rho_{el,id} = 77$ e.u. nm^{-3} for the ideal contrast of pure PVDF. In particular, the elevated contrast of sample CPvi can only be explained if it is assumed that the plasticizer mixes with the amorphous phase, decreasing its electron density. The contrast of the transparent sample is close to the ideal contrast of pure PVDF. Therefore it is assumed that most of the plasticizer has been lost during ageing.

4.4.5. *The 1D scattering curve in the vicinity of zero.* If it is assumed that the layers in the stacks are sufficiently flat and extended, the shape of $\tilde{I}_{id}(s)/V$ in the vicinity of zero is predictable from the results of the IDF analysis (5). From the IDF analysis, the virgin sample has considerable roughness of the layer surfaces and the corresponding scattering cannot be separated from the scattering of the semi-crystalline stacks. This is also true for the aged translucent sample CPT. However, since here the surface roughness effect could, to some extent be separated, comparison appears to be meaningful. Utilizing (5) one computes (17×10^3 e.u. nm^{-4}), almost exactly the value of the measured (18×10^3 e.u. nm^{-4}) slope, but the measured intercept (2500 e.u. nm^{-5}) is more than double the computed one (930 e.u. nm^{-5}).

Even if the layers are assumed to be sufficiently flat and extended, such a difference can be explained by the interaction of surface roughness and voids in scattering data. A complete separation of the surface roughness would lower $\tilde{A}_P$ by 4% and increase the average crystalline thickness by 0.5 nm. The computed slope would increase by 30% and the intercept by 20%. The remaining contribution in the scattering curve of the sample CPT could easily be interpreted in terms of yet undiscovered voids.

For both the white samples of aged material, the void content is so high that no information about the stacks from crystalline and amorphous lamellae can be obtained from the central part of their scattering curves. The similarity of all the WAXS patterns as well as the identity of the SAX tails implies that the semi-crystalline topology of all the aged samples is essentially the same. Under the assumption that sample CPT does not contain any voids and that all voids in the white samples contribute to the observed void scattering, the volume fraction of voids, $v_{void} \simeq Q_{void}/\rho_{el}^2$, can be calculated. For the white samples, from their excess scattering power, Q_{void}, and the average electron density of the samples $\rho_{el} \simeq 500$ e.u. nm^{-3}, void fractions of 0.16% for CPT and 0.72% for CPO are calculated.

5. Conclusions

A practical application of detailed analysis of absolute small-angle X-ray data is the study of 'impure' industrial materials and their ageing by an environment. While the creation of voids could have been inferred from visual inspection of the aged material, the SAXS method has shown a probable cause for the emergence of those voids, namely the collapse of the amorphous layers due to plasticizer loss.

For the special topology of stacked layers, the extended linear shape of slit-smeared one-dimensional SAXS curves follows from theoretical consideration (Stribeck, 1996). Experiments suggest that void scattering appears not to alter this principle. If this is true, void content can simply be evaluated from the initial slope of the smeared 1D SAXS curve. If the void content increases during service time this means that the aged state of the sample can be determined from the initial slope of this scattering curve.

References

Arnold, C. Jr, Leo, A. & Tarjani, M. (1988). *Polym. Mater. Sci. Eng.* **59**, 18–22.

Blundell, D. J. (1978). *Polymer*, **19**, 1258–1265.

Hermans, J. J. (1944). *Recl Trav. Chim. Pays-Bas*, **63**, 211–218.

Johansson, A. & Tegenfeldt, J. (1993). *Solid State Ion.* **67**, 115–121.

Montserrat, S. & Cortes, P. (1995). *J. Mater. Sci.* **30**, 1790–1793.

Perret, R. & Ruland, W. (1971). *J. Appl. Cryst.* **4**, 444–451.

Ruland, W. (1977). *Colloid Polym. Sci.* **255**, 417–427.

Ruland, W. (1987). *Macromolecules*, **20**, 87–93.

Semenov, A. N. (1994). *Macromolecules*, **27**, 2732–2735.

Stabinger, H. & Kratky, O. (1978). *Macromol. Chem.* **179**, 1655–1659.

Stribeck, N. (1993). *Colloid Polym. Sci.* **271**, 1007–1023.

Stribeck, N. (1996). *Macromolecules*, **29**, 7217–7220.

Vonk, C. G. & Kortleve, G. (1967). *Colloid Polym. Sci.* **220**, 19–24.

Yampol'skii, Yu. P., Shishatskii, S. M., Shantorovich, V. P., Antipov, E. M., Kuzmain, N. N., Rykov, S. V., Khodjaeva, V. & Plate, N. A. (1993). *J. Appl. Polym. Sci.* **48**, 1935–1944.

Zernike, F. & Prins, J. A. (1927). *Z. Phys.* **41**, 184–194.